ESI

The interlocked *in-situ* fabrication of Graphene@Prussian Blue nanocomposite as high-performance supercapacitor

Shi-Cheng Wang, Minli Gu, Luqing Pan, Junfeng Xu, Lei Han and Fei-Yan Yi*

School of Materials Science & Chemical Engineering, Ningbo University, Ningbo, Zhejiang 315211, China. E-mail: yifeiyan@nbu.edu.cn

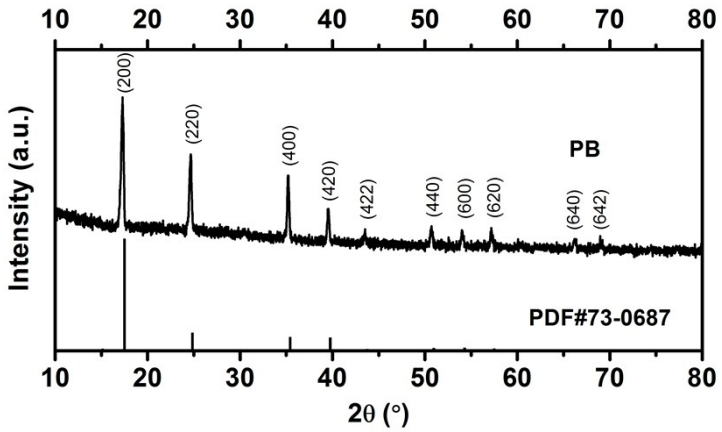

Fig. S1 XRD patterns of PB nanocubes.

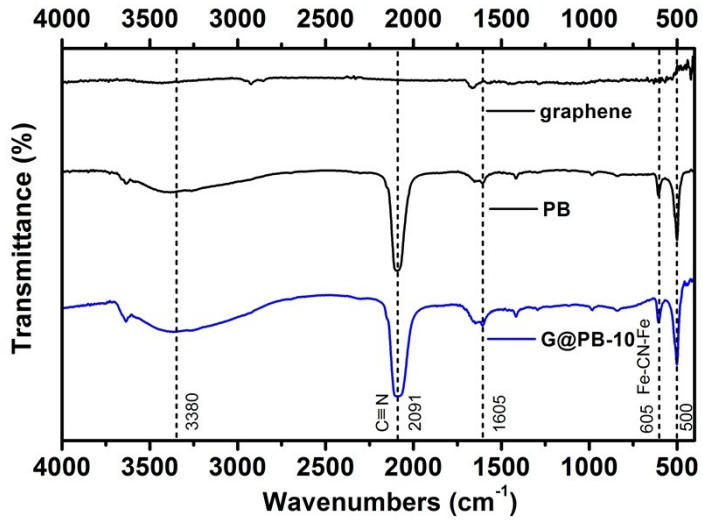

Fig. S2 FT-IR spectra of graphene, PB and G@PB-10.

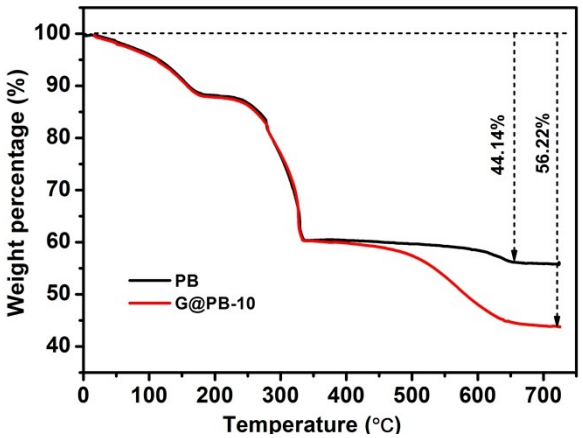

Fig. S3 TGA curves of PB and G@PB-10.

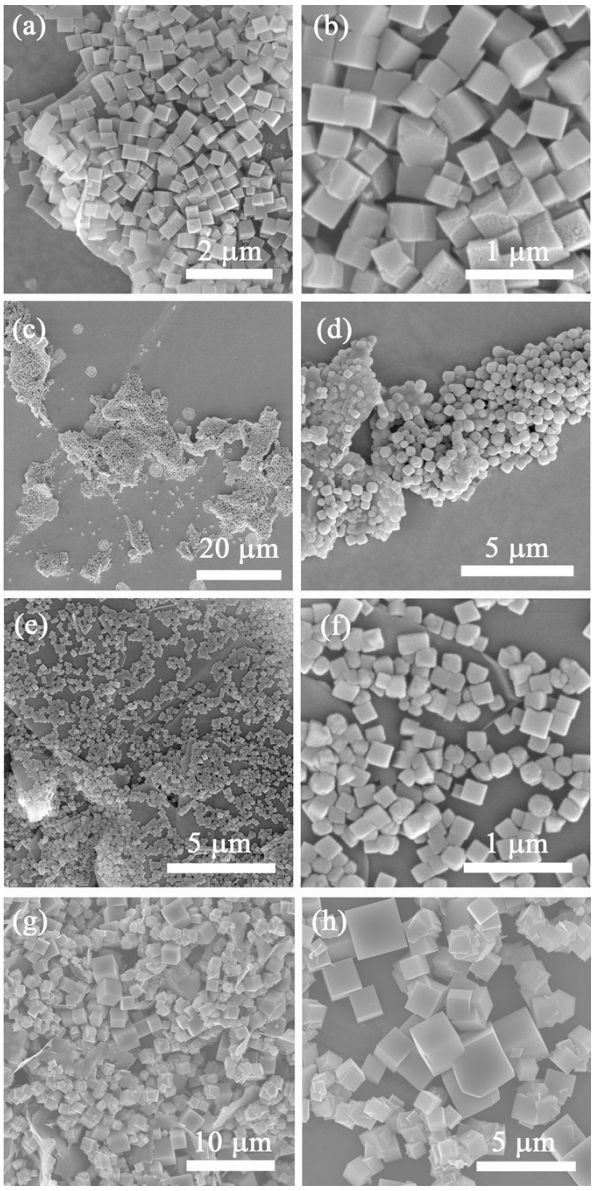

Fig. S4 SEM images of (a-b) G@PB-1, (c-d) G@PB-5 and (e-f) G@PB-10 nanocomposites at different magnifications. (g,h) The SEM images of G@PB-5 synthesized in the absence of PVP.

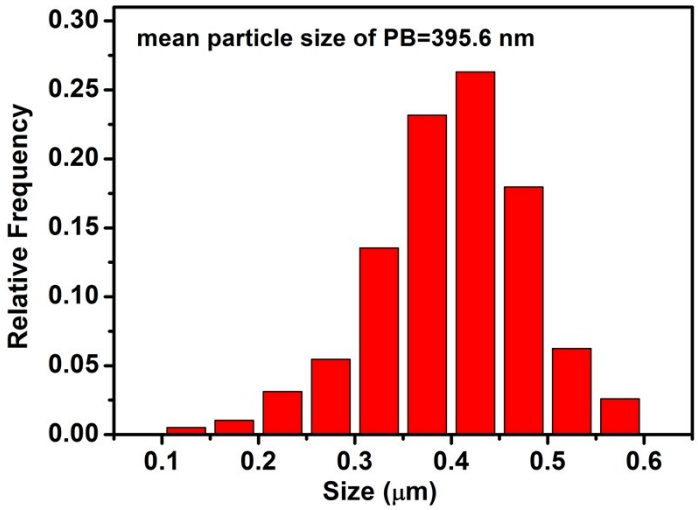

Fig. S5 Size distribution histogram of PB nanocubes covered on the surface of graphene according to the SEM image of G@PB-5 nanocomposites (Fig 2d).

Size of each nanocube was calculated one by one using the tool of Nano Measure software availably. Histogram was constructed by grouping their sizes to different intervals, and mean particle size and relative frequency were determined by counting as many as 384 particles to minimize errors

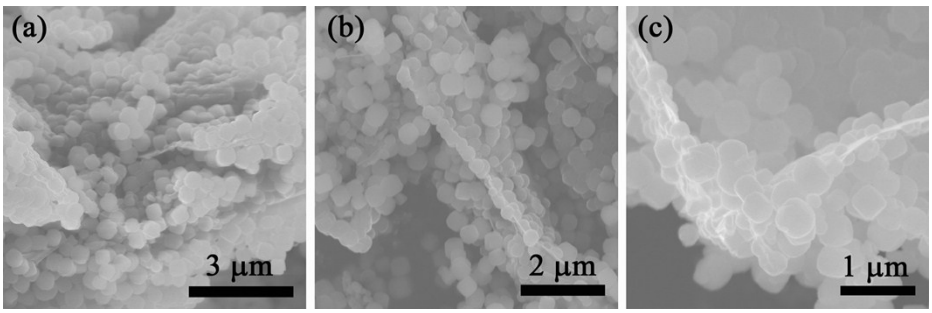

Fig. S6 SEM images of G@PB-5 nanocomposites which indicates that PB growing on the both sides of graphene sheets.

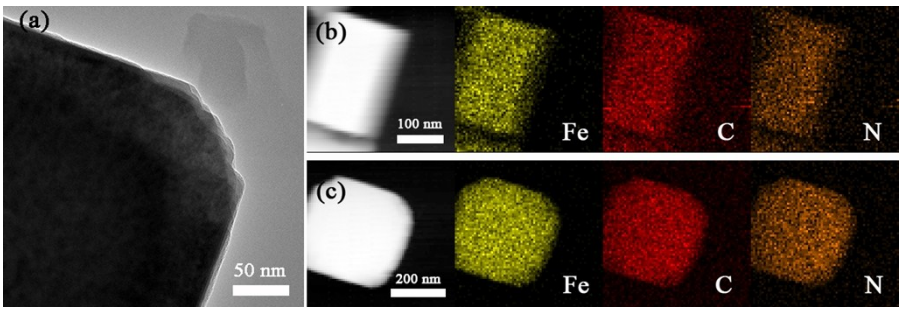

Fig. S7 (a) TEM image of a corner of PB nanocube in G@PB-5. (b-c) HAADF-STEM image and STEM-EDS mapping images of PB and G@PB-5 showing the uniform distribution of Fe, C and N.

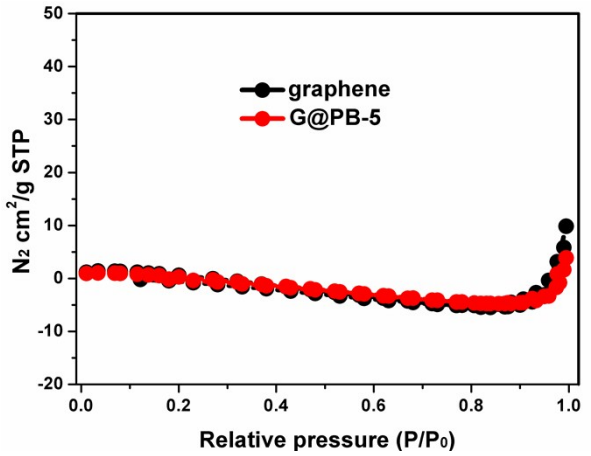

Fig. S8 The N_2 adsorption desorption isotherm curves of pristine graphene and G@PB-5 samples.

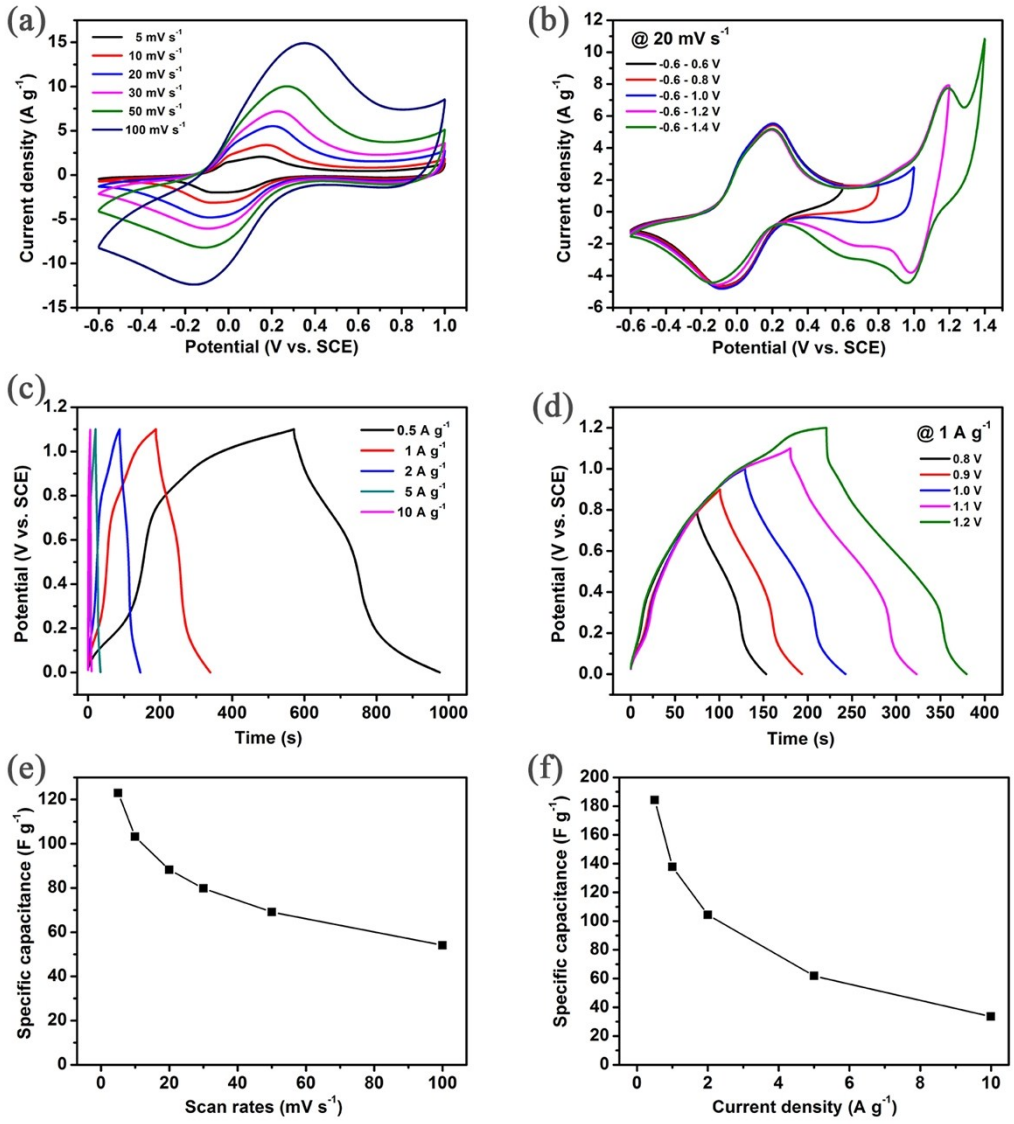

Fig. S9 (a) CV curves of pure PB at different scan rates. (b) CV curves of pure PB at a scan rate of 20 mV s^{-1} with different potential window. (c) GCD curves of pure PB at different current densities. (d) GCD curves of pure PB at a current density of 1 A g^{-1} with different potential

window. (e-f) The corresponding specific capacitance of PB electrode calculated by CV curves and GCD curves.

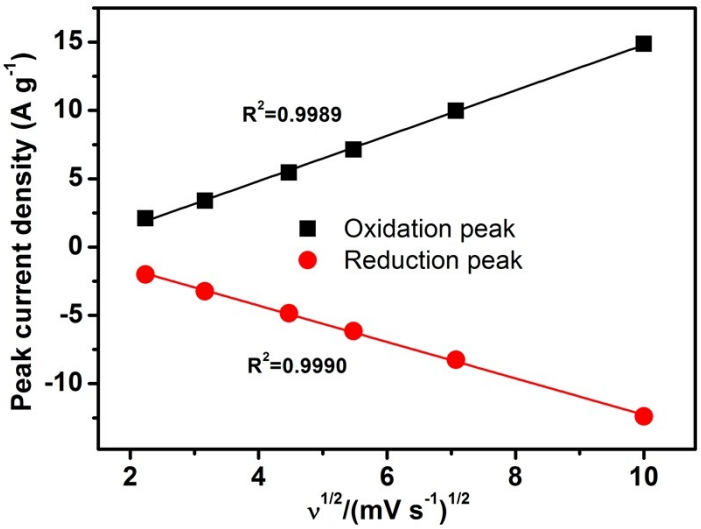

Fig. S10 Redox peak current densities as a function of the square root of the scan rate of pure PB.

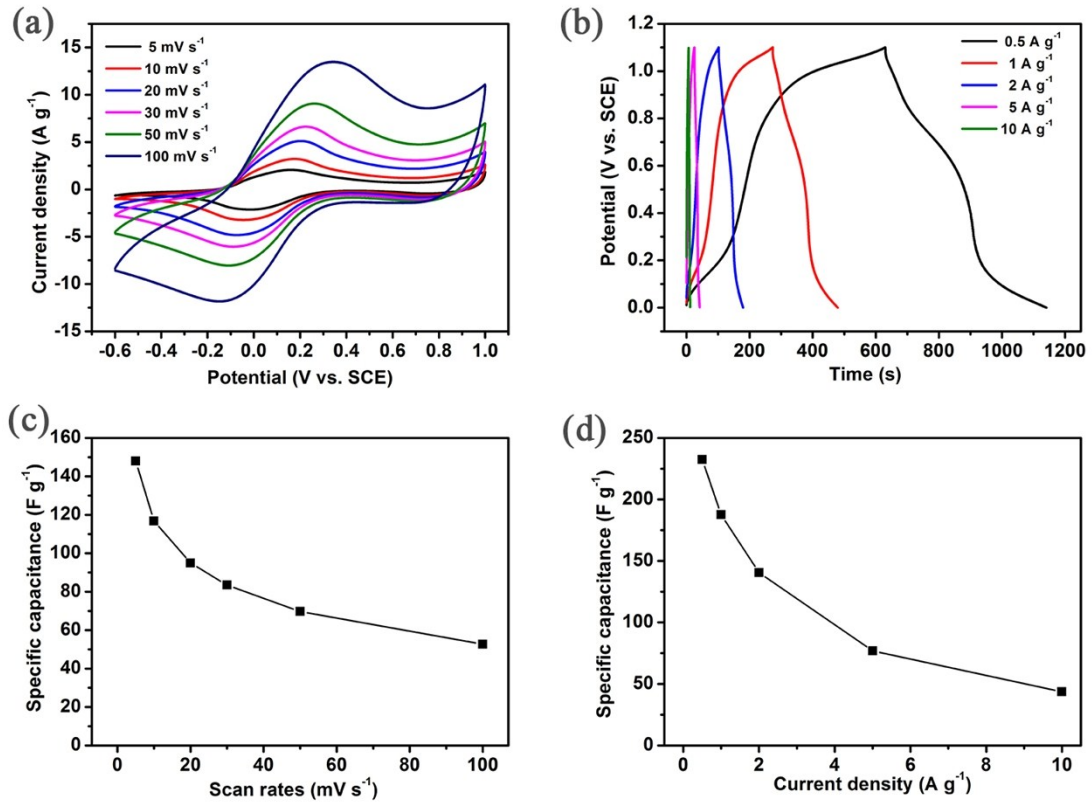

Fig. S11 (a) CV curves of G@PB-1 at different scan rates. (b) GCD curves of G@PB-1 at different current densities. (c-d) The corresponding specific capacitance of G@PB-1 electrode calculated by CV curves and GCD curves.

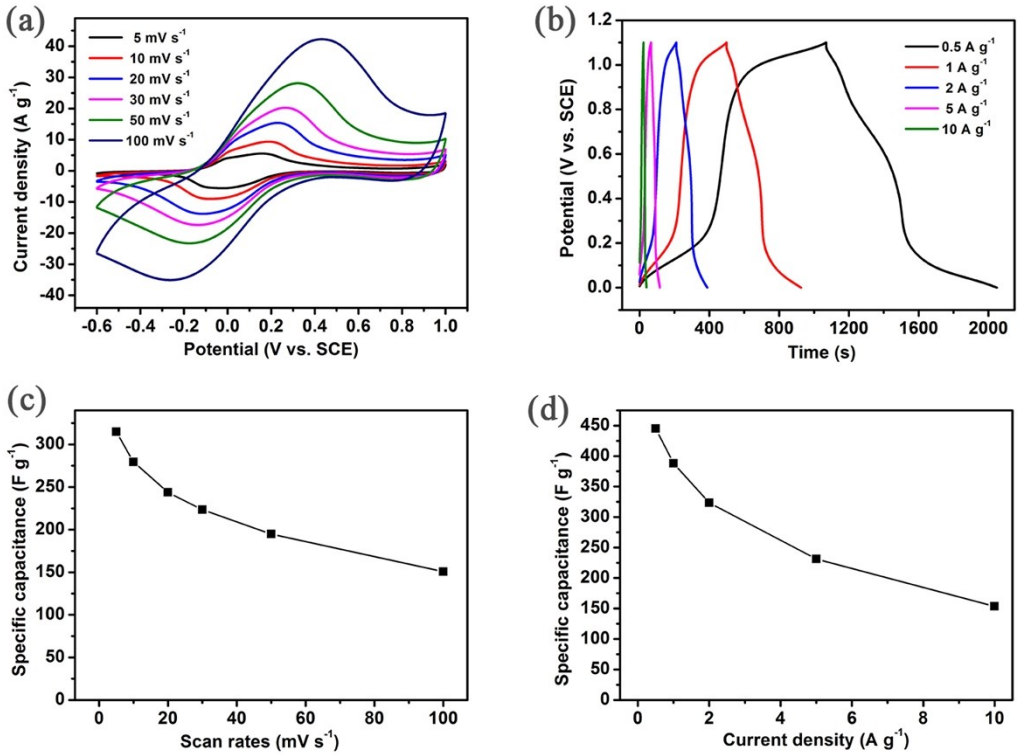

Fig. S12 (a) CV curves of G@PB-5 at different scan rates. (b) GCD curves of G@PB-5 at different current densities. (c-d) The corresponding specific capacitance of G@PB-5 electrode calculated by CV curves and GCD curves.

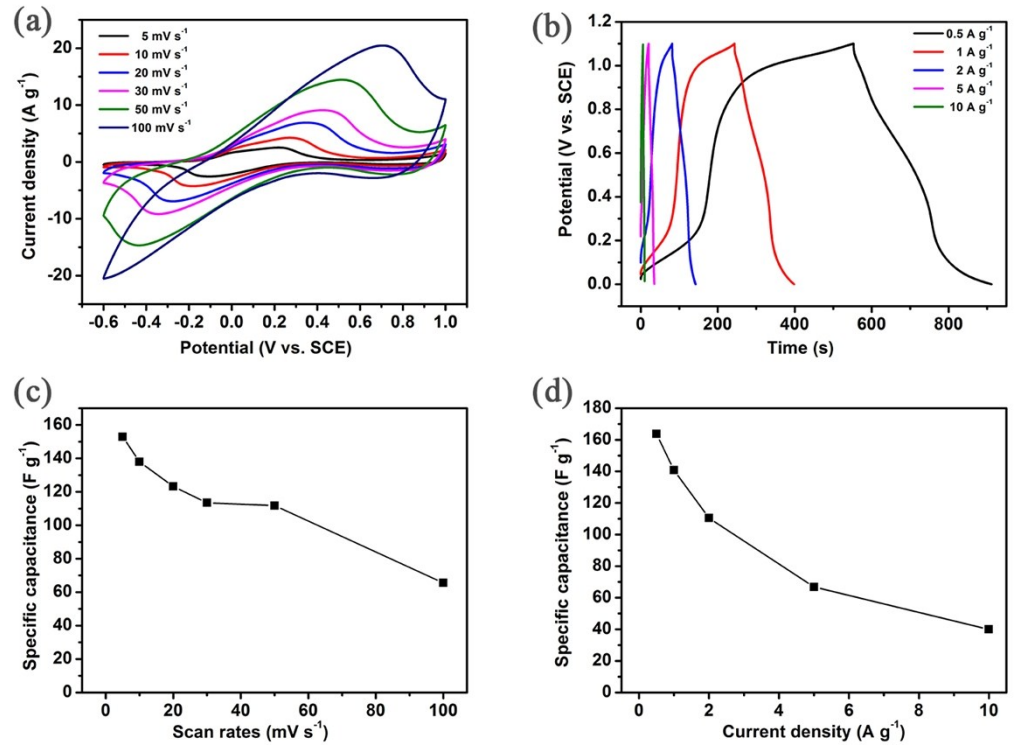

Fig. S13 (a) CV curves of G@PB-10 at different scan rates. (b) GCD curves of G@PB-10 at different current densities. (c-d) The corresponding specific capacitance of G@PB-10 electrode calculated by CV curves and GCD curves.

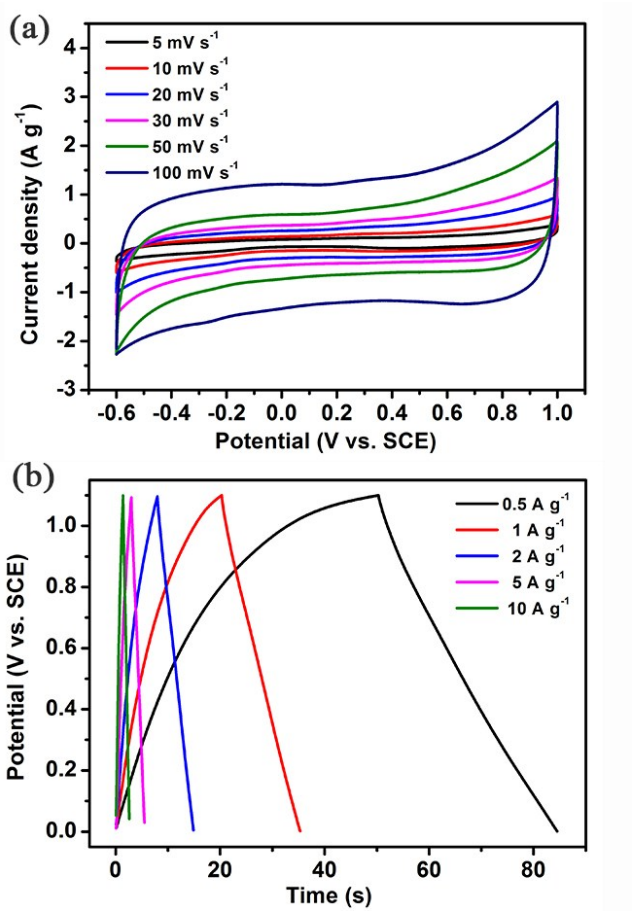

Fig. S14 (a) CV curves of graphene at different scan rates. (b) GCD curves of graphene at different current densities.

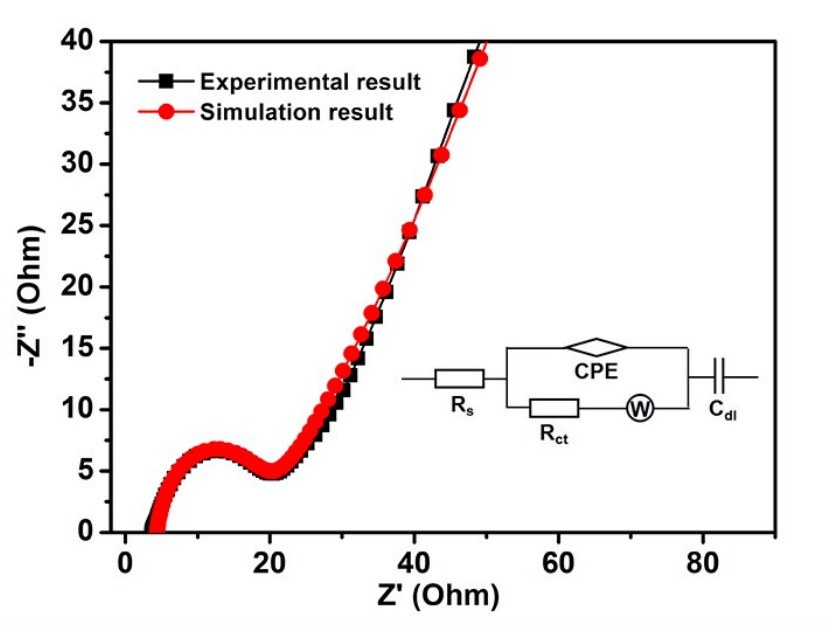

Fig. S15 Nyquist plots of the experiment data and the simulation result of PB electrode.

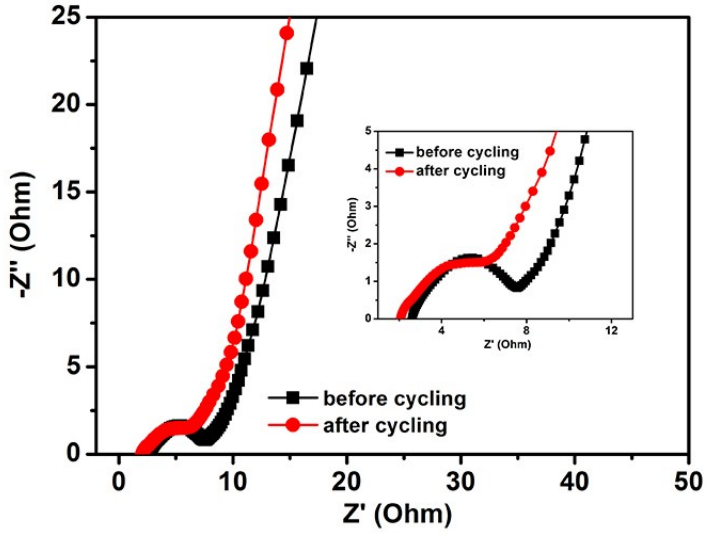

Fig. S16 Nyquist plots of the G@PB-5 electrode before and after 5000 charge-discharge cycles. The insert shows the impendance in the high freguency region of the electrode.

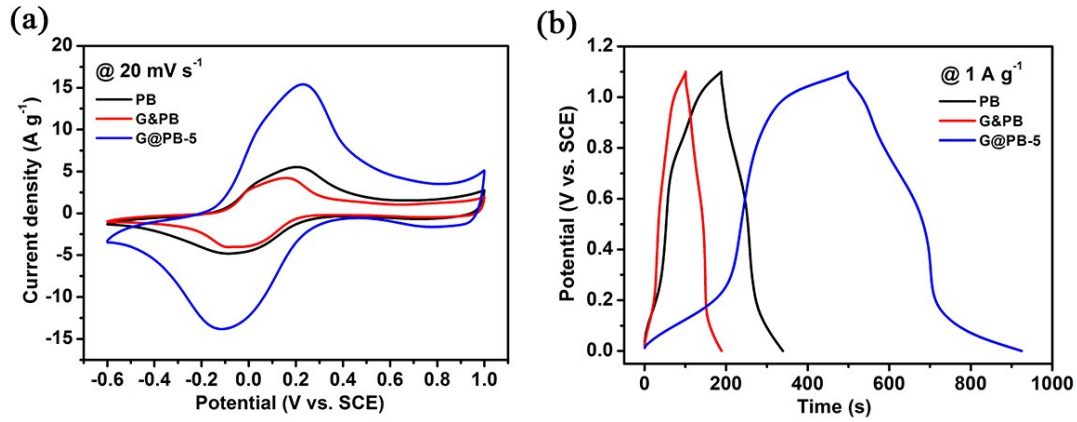

Fig. S17 (a) CV curves of PB, G&PB, G@PB-5 at a scan rate of 20mV s^{-1}. (b) GCD curves of PB, G&PB, G@PB-5 at a current density of 1 A g^{-1}.

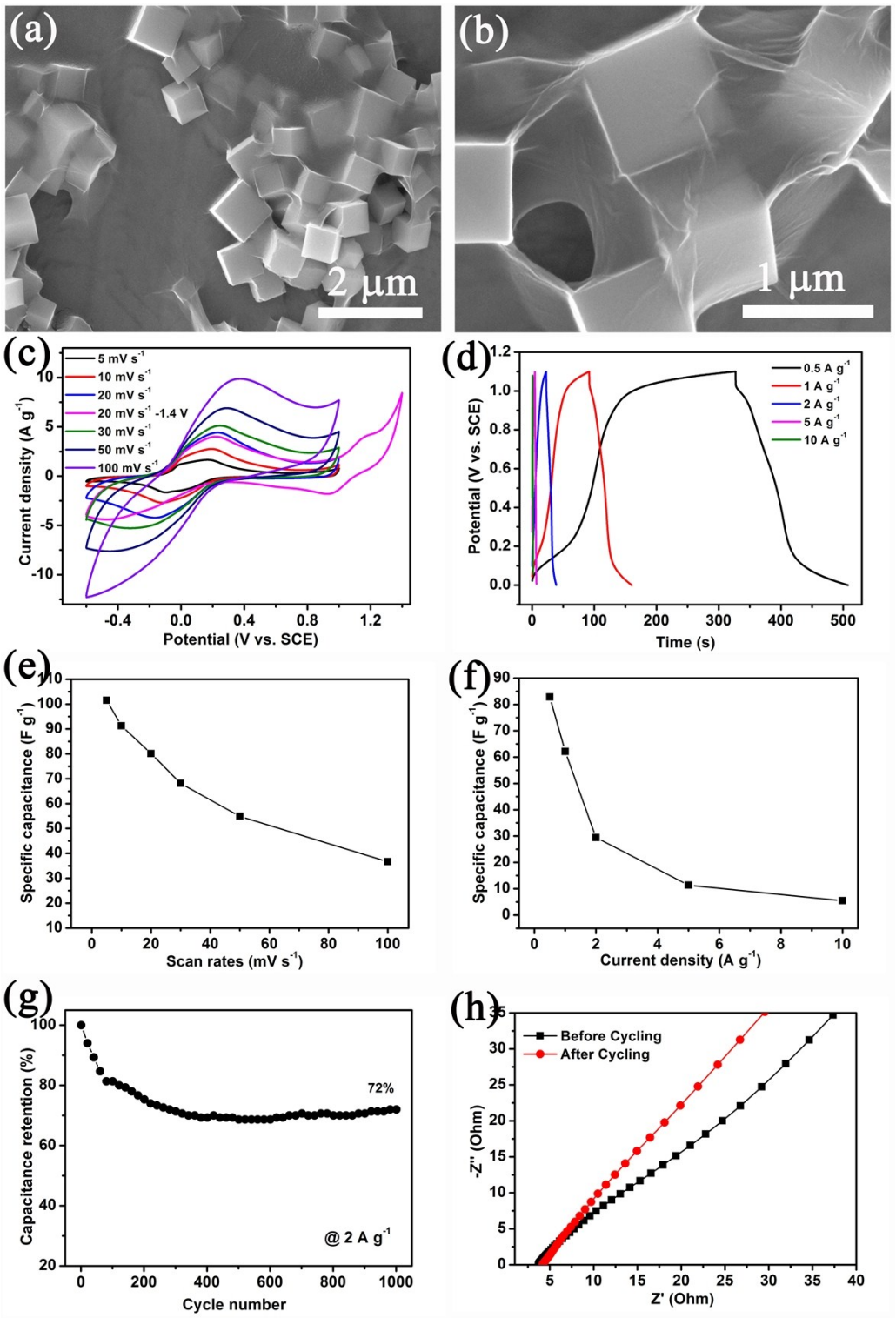

Fig. S18 (a-b) SEM images of GO/PB hybrid composites at different magnifications. (c) CV curves of GO/PB at different scan rates. (d) GCD curves of GO/PB at different current densities. (e-f) The corresponding specific capacitance of GO/PB electrode calculated by CV curves and GCD curves. (g) Cycling performance of GO/PB at a current density of 2 A g^{-1}. (h) Nyquist plots of the GO/PB electrode before and after 1000 charge-discharge cycles. GO/PB electrode exhibits a specific capacitance of 101.51 F g^{-1} at 5 mV s^{-1} and 82.86 F g^{-1} at 0.5 A g^{-1}. And its capacitance retention are 36.1% from 5 to 100 mV s^{-1} and 6.6% from 0.5 to 10 A g^{-1}. Its cycle stability curves

and Nyquist plots before and after 1000 charge-discharge cycles also indicate a low stability.

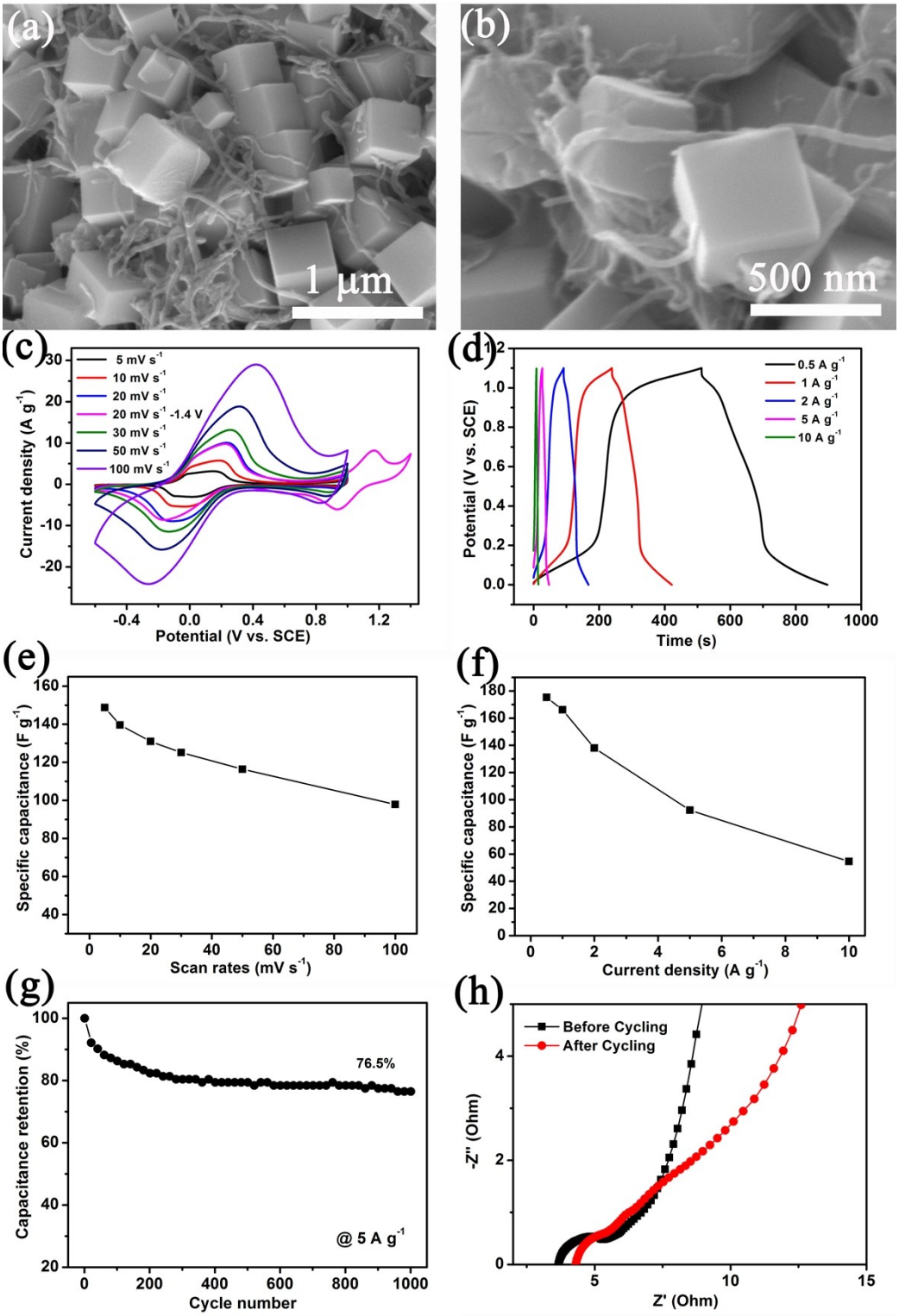

Fig. S19 (a-b) SEM images of MCNTs/PB hybrid composites at different magnifications. (c) CV curves of MCNTs/PB at different scan rates. (d) GCD curves of MCNTs/PB at different current densities. (e-f) The corresponding specific capacitance of MCNTs/PB electrode calculated by CV curves and GCD curves. (g) Cycling performance of MCNTs/PB at a current density of 5 A g^{-1}. (h) Nyquist plots of the MCNTs/PB electrode before and after 1000 charge-discharge cycles.

MCNTs/PB electrode exhibits a specific capacitance of 148.74 F g^{-1} at 5 mV s^{-1} and 175.23 F g^{-1} at 0.5 A g^{-1}. And its capacitance retention are 65.8% from 5 to 100 mV s^{-1} and 31.1% from 0.5 to 10 A g^{-1}. Its cycle stability curves and Nyquist plots before and after 1000 charge-discharge cycles also mainfest a low stability.

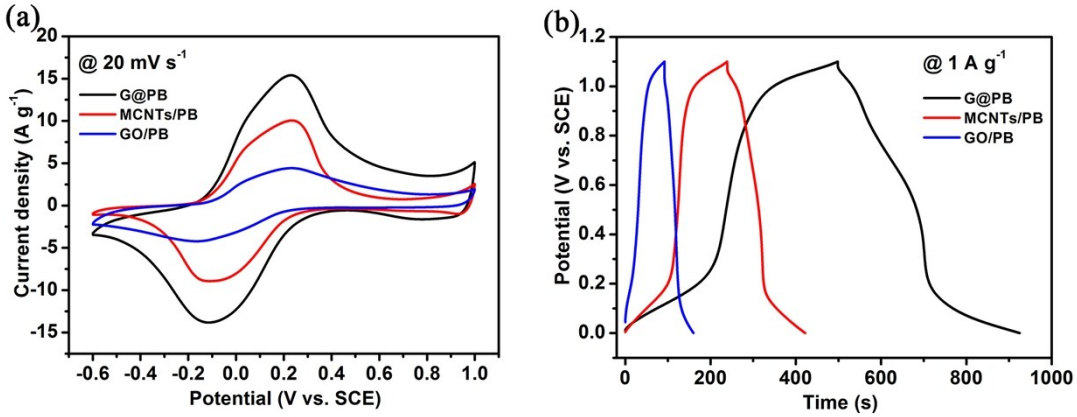

Fig. S20 (a) CV curves of G@PB, MCNTs/PB and GO/PB at a scan rate of 20 mV s^{-1}. (b) GCD curves of G@PB, MCNTs/PB and GO/PB at a current density of 1 A g^{-1}.

Table. S1 Comparison of the electrochemical performance of PB and various PB/carbonaceous material composites.

sample	Electrolyte	[b]SC (F g^{-1})	[a]CD	[c]CR	Ref.
PB	0.5 M Na_2SO_4	107	0.5 A g^{-1}	100% (1100 cycles)	[1]
PB/rGO	1 M KNO_3	251.6	10 mV s^{-1}	92% (1000 cycles)	[2]
G-rGO-PB	0.1 M KCl	385	1 A g^{-1}	94% (1000 cycles)	[3]
PPy-PB-GO	1 M KNO_3	525.4	5 A g^{-1}	96% (2000 cycles)	[4]
graphene@PB	**0.5 M Na_2SO_4**	**388.09**	**1 A g^{-1}**	**97.2% (5000 cycles)**	**This work**
GO-PB	0.5 M Na_2SO_4	82.86	1 A g^{-1}	72% (1000 cycles)	This work
MCNTs-PB	0.5 M Na_2SO_4	175.23	1 A g^{-1}	76.5% (1000 cycles)	This work

[a] CD: current density.

[b] SC: specific capacitance.

[c] CR: capacitance retain.

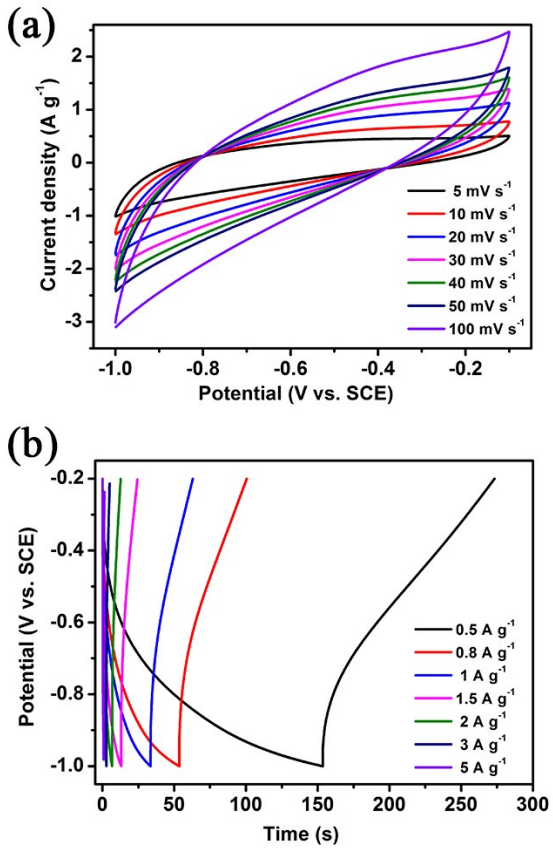

Fig. S21 (a) CV curves of AC at different scan rates. (b) GCD curves of AC at different current densities.

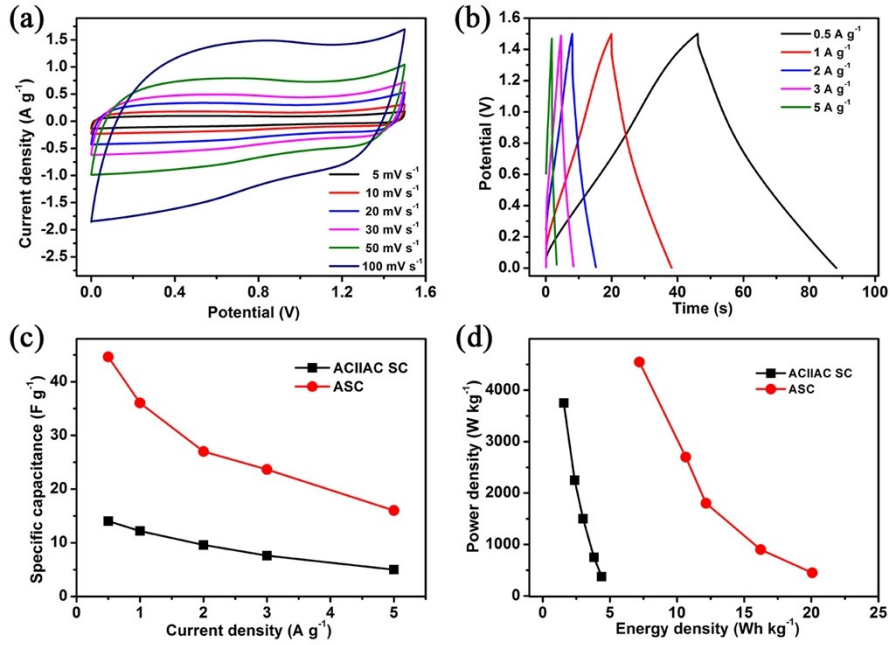

Fig. S22 (a) CV curves of AC//AC SC at different scan rates. (c) GCD curves of AC//AC SC at different current densities. (d) The corresponding specific capacitance of AC//AC SC calculated by GCD curves compared to G@PB-5//AC ASC. (e) Ragone plots of AC//AC SC compared to G@PB-5//AC ASC.

References

[1] L. Zhou, Z. Yang, C. Li, B. Chen, Y. Wang, L. Fu, Y. Zhu, X. Liu and Y. Wu, *Rsc adv.*, 2016, **6**, 109340-109345.

[2] M. Luo, Y. Dou, H. Kang, Y. Ma, X. Ding, B. Liang, B. Ma and L. Li, *J. Solid State Electrochem.*, 2015, **19**, 1621-1631.

[3] M. Zhang, C. Hou, A. Halder, J. Ulstrup and Q. Chi, *Biosens. Bioelectron.*, 2017, **89**, 570-577.

[4] Y. Zou, Q. Wang, C. Xiang, Z. She, H. Chu, S. Qiu, F. Xu, S. Liu, C. Tang and L. Sun, *Electrochim. Acta*, 2016, **188**, 126-134.